AUTOMATED TRACKING OF 2D AND 3D ICE RADAR IMAGERY USING VITERBI AND TRW-S

Victor Berger[1], Mingze Xu[2], Shane Chu[1], David Crandall[2], John Paden[1], Geoffrey C. Fox[2]

[1]Center for Remote Sensing of Ice Sheets, University of Kansas, USA
[2]School of Informatics, Computing, and Engineering, Indiana University, USA

ABSTRACT

We present improvements to existing implementations of the Viterbi and TRW-S algorithms applied to ice-bottom layer tracking on 2D and 3D radar imagery, respectively. Along with an explanation of our modifications and the reasoning behind them, we present a comparison between our results, the results obtained with the original implementations, and those obtained with other proposed methods of performing ice-bottom layer tracking.

Index Terms— Glaciology, radar tomography, ice thickness, ice-bottom tracking, image classification

1. INTRODUCTION

Ground-penetrating radar devices, such as the Multichannel Coherent Radar Depth Sounder (MCoRDS) [1] system, are able to map the underground anatomy of icy regions of the globe such as Greenland and Antarctica. The ice-bed topography data acquired by these devices allow for research regarding the variations in polar ice thickness and are factored into modelling the contribution of polar regions to sea level.

The generated imagery of the subterranean ice structures includes the interfaces between air and ice (ice-surface) and between ice and bedrock (ice-bottom), from which measurements such as ice thickness can be derived. While these interfaces are usually clearly identifiable in the 2D and 3D echograms, the large amount of data makes it impractical for these to be analyzed and labeled manually. Thus arises the need for an automated system of detecting these interfaces at a high level of accuracy and in a timely fashion.

This problem has received attention from researchers such as Gifford *et al.* [2], who proposed edge-based and active-contour-based iterative methods of tracking the interfaces. Similarly, a solution utilizing a level-set technique was suggested by Rahnemoonfar *et al.* [3].

Another approach was proposed by Crandall *et al.* [4], which poses this tracking as an inference problem, solved using the Viterbi algorithm on a probabilistic graphical model which combines several known constraints of the polar ice layers. An improved solution using a similar model was suggested by Lee *et al.* [5], which employed a Markov Chain Monte Carlo (MCMC) technique. This problem was later revisited by Xu *et al.* [6], using a sequential tree-reweighted message passing (TRW-S) [7] technique.

In this paper we describe modifications made to the aforementioned solutions proposed by Crandall and Xu, including the incorporation of further domain-specific knowledge to the cost-functions and general application of the algorithms, which allows for improved results.

In our work, we make the assumption that the air-ice interface is known *a priori*, since there exist accurate surface estimates (such as ArcticDEM and Bedmap2 [8]) based on satellite imagery, and thus we focus on locating only the ice-bedrock interface. We also assume that each interface is single valued, meaning that it can take on only one value for each column in the imagery; in other words, there are no overhangs or cave-like features.

The organization of this paper is the following: in Section 2, we present background information regarding the 2D and 3D data, the two algorithms used, and how the interface tracking is performed. In Section 3, we present our modifications to the original solutions, explaining the rationale behind these changes. In Section 4, we present our results and compare those with the ones obtained by the aforementioned authors. We also offer a comparison between our results and the available manually-tracked ground-truth data.

2. BACKGROUND

2.1. 2D and 3D imagery

After a series of signal and array processing techniques are applied on the data collected by the aforementioned radar systems, two types of imagery of the underground ice topography can be generated: 2D echograms which display the subterranean ice structures along the flight profile, and 3D images that represent a sequence of cross-track images (or "slices") of the terrain. While specific details on the processing techniques fall outside the scope of this work, further information can be obtained from [9] and [10].

In the 2D echogram imagery, the horizontal axis of the image represents the along-track dimension, while the y-axis depicts the fast-time dimension, containing information about the depth of the subterranean structure in the nadir direction.

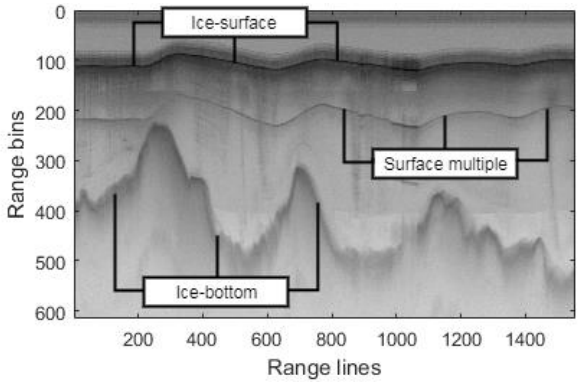

Fig. 1. 2D echogram from data captured by MCoRDS.

See Fig. 1 for an example. The surface multiple and other clutter (unwanted scattering) complicate the image tracking process.

Each slice in the 3D image presents the targets across all elevation angles, with the horizontal axis representing the elevation angle and the vertical axis representing the fast-time dimension. Fig. 2 shows a single representative slice from a 3D image. In the 3D tracking problem, for each slice, there is a manually picked range bin for column 33 which [6] refers to as the *bottom bin*. This is indicated by the red 'x'.

While both of these formats of radar imagery display information about the underground ice-bed topography of the area, one of the fundamental differences is that there exists a strong correlation between consecutive 3D slices, as they represent adjacent cross-sections of the surveyed terrain. On the other hand, no similar "third dimension" is available for the 2D echograms.

This difference between the two cases generates the need for two separate algorithms that can take advantage of the specific constraints and requirements of each situation.

2.2. A graphical model for layer-tracking

In the work of Crandall *et al.* [4] and Xu *et al.* [6], polar echogram layer-tracking is posed as an inference problem on a statistical graphical model. In both scenarios, the authors formulate a Markov Random Field (MRF) framework constructed from the assumptions and the known constraints of the data. In both cases, the hidden states are the rows that correctly label the ice-bedrock interface in each column of the image matrix.

While the method of performing inference on the MRF and ultimately detecting the highest-probability (lowest-cost) solution differs between the two solutions, the probability of transitioning between columns of the image matrix is modelled in a similar manner. These terms are calculated from two cost functions, one unary and the other binary.

The unary cost ψ_U is calculated for every pixel of the image matrix. From [6], $\psi_U = \psi^{temp} + \psi^{air} + \psi^{bin}$, where ψ^{temp} accounts for pixel intensity, ψ^{air} ensures the bottom is beneath the surface and pushes the bottom away from the

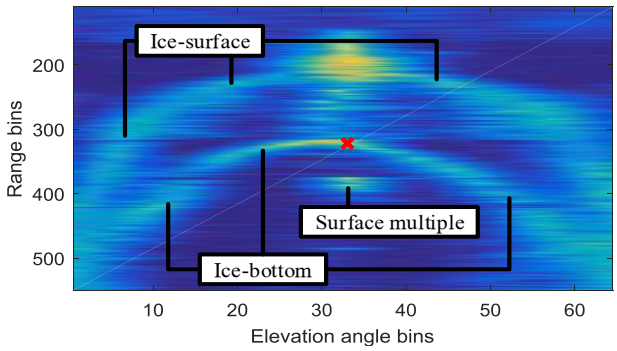

Fig. 2. A slice from 3D imagery from data captured by MCoRDS.

surface, and ψ^{bin} ensures the bottom layer is below the *bottom-bin* and is only applicable to the 3D imagery.

The binary term ψ_B is based on the cost of moving from one column to the next, as a square of the absolute distance between the rows of the two columns. The square term corresponds to a log Gaussian distribution. In other words, there is an increased cost of "jumping" more rows when moving from the current column to the next – this effectively enforces a smoothness constraint on the model. A smooth interface is generally a reasonable assumption for the bottom of the ice sheet.

2.2. 2D imagery and the Viterbi algorithm

The Viterbi algorithm is an efficient method of finding the highest-probability (or lowest-cost) sequence of hidden states in a discrete-time Markov process. With the aforementioned unary and binary cost information, the Viterbi algorithm can be tasked with finding the set of column-to-column transitions that produces the lowest global cost of labeling the ice-bedrock interface.

2.3. 3D imagery and the TRW-S algorithm

In order to take advantage of the strong correlation between consecutive slices of three-dimensional imagery, Xu *et al.* [6] proposes the use of a sequential tree-reweighted message passing (TRW-S) [7] technique, in which cost information is passed both intra- and inter-slice.

While the intra-slice message passing procedure performs in similar fashion to the Viterbi algorithm applied on 2D images, the inter-slice message passing propagates ice-bottom layer evidence between consecutive slices of 3D imagery, increasing the likelihood to successfully converge towards it.

Unlike the Viterbi algorithm, which is guaranteed to return the global maximum likelihood path of an HMM, the TRW-S algorithm on an MRF is not guaranteed to converge to a global optimum. However, based on trial and error, we found that 50 iterations usually produces satisfactory results. More systematic testing in the future may suggest convergence criteria rather than a fixed number of iterations.

3. MODIFICATIONS

3.1. Modifications applicable to both 2D and 3D imagery

We modified the template term to deal with the wide dynamic range of the images. In [4] and [6], ψ^{temp} measures the squared difference in the image pixel intensity relative to a template found through an automated training sequence using the *a priori* surface information. Although it is data dependent, the template invariably has a peak in the center with decreasing values towards the edges of the template. This means that a peak response of a *similar* intensity will produce the lowest cost. The issue with using the squared distance to the template is that the peak intensity from the ice bottom layer varies with larger intensities generally indicating a better measurement (since these correspond to greater signal to noise ratios). To better represent peak intensity variability, we now use a correlation operation that multiplies the template with the image:

$$\psi^{temp}(s \mid I) = -\sum_{p \in T} I(s+p)\mu_p$$

where $p \in T$ are the pixels in the template (fixed to include the 5 pixels above and below pixel of interest s) and μ_p is the template peak function fixed to $\text{sinc}\left(\frac{5p}{1.5}\right)$ which for ±5 pixels corresponds roughly to the midpoint in the first minimum on either side of the sinc function peak at $p = 0$. To deal with varying intensities, [6] thresholded the images to a fixed value. Aside from the issue of needing to set this threshold optimally on a case to case basis, this meant that strong peaks would get clipped. This clipping led to inaccurate tracking of strong returns and since the correlation method deals well with varying intensities, the thresholding was removed.

Previously, the algorithms did not have a method to remove boundary pixels. For the 3D imagery, the edges of each slice tend to be very blurry and low quality even for relatively clear images as shown in Fig. 2. Although, the dynamic β_j weight in [6] partially accounts for this, we found it more effective to just remove these pixels entirely from the calculation.

The previous ψ^{bin} term simply forced the bottom surface to fall beneath the manually picked *bottom-bin*. However, the *bottom-bin* was more likely to be centered on the correct bottom surface than to always be above it. For this reason, we modified this to require the bottom to be ±20 pixels of the bottom-bin.

Where the bottom and surface merge, the tracking algorithms generally do poorly because the ψ^{air} term does not allow the layers to merge. Since points where the bottom and surface merge correspond to no ice and "ice mask" datasets exist [8,9] that map these no ice locations, [6] introduced a ψ^{extra} cost term which forces the two surface and bottom layers to merge where there is no ice.

Unlike [6] which had a binary transition between ice and no-ice, we modified the cost to enforce a smooth transition between ψ^{air} and ψ^{extra} for non-icy and icy areas respectively. The transition follows the square of the distance between a given pixel and neighboring bins with no ice. With this term, the algorithm is encouraged to draw the bottom layer towards the surface near regions of no-ice.

For each elevation angle in the 3D image, the *a priori* surface DEM from ArcticDEM is used to find an estimate of the range-time to the ice-surface. Aside from providing the surface location, it is used to 1) extract image intensity properties of the surface scattering that are used to track the unknown ice-bottom and 2) to perform a rough calibration of the radar steering vectors by adjusting the radar-estimated DoA to match the surface-DEM-derived DoA. The averaged adjustment is then applied to the ice bottom for which there is no *a priori* information.

In [4] and [6], the ψ_B term, that controls smoothness, assumes a flat surface in the image. However, for 2D imagery the ice surface correlates to the ice bottom and so a bias was added to the ψ_B term to center the distribution to match the surface slope. For the 3D slices which are actually in polar coordinates (elevation angle is one axis), a flat surface actually shows up curved as shown by the "flat" ice surface in Fig. 2. Because of this expected curvature, we added the same adjustment to encourage the bottom slope to track the surface slope in the 3D algorithm.

In order to find specific weights for the aforementioned variables, we have employed the Random Search [12] hyper-parameter optimization technique.

3.2. Modifications applicable to 2D imagery

Although ground-truth is available from crossing flight lines that have already been tracked (usually from past seasons), previous tracking solutions did not make use of this information. Using the Open Polar Server [13], we extract the ice-bottom location at all the crossovers. We then use these existing layer points as ground-truth to our algorithm.

Additionally, previous efforts divided flights into small data frames for processing. These data frames are contiguous and this sometimes resulted in lower quality results near the edges of the data frames than is possible by processing the entire flight. This also helps increase the probability that a cross over flight will include ground truth, although this is not strictly necessary for the algorithm to perform well.

Although [6] used the ice mask for 3D imagery, the 2D algorithms did not make use of the ice mask. We have incorporated the ice mask evidence into the 2D image tracker.

Since the 2D imagery intensity exhibits a strong dependence on depth in ice due to the ice loss and spherical spreading loss, we apply a simple detrending routine that normalizes the mean intensity of each row. This substantially helps the tracker in areas where the bed echo is weak. Without this normalization, clutter near the surface is often so strong that the bottom layer tracker jumps up to this very strong clutter signal despite the smoothness constraint.

One source of clutter that is predictable is the ice-surface multiple, which can act as a false-positive (see Fig. 1). The multiple is caused by ringing of the radar signal between the

aircraft and the surface. We have incorporated a simple method of automatically reducing the image intensity of pixels located around the area corresponding to the surface multiple by using the first surface return to estimate and remove the surface multiple ringing.

3.3. Modifications applicable to 3D imagery

TRW-S passes a cost message between each pixel and its neighbors to the left and right (elevation angle dimension) and forward and backward (along-track dimension) in every loop iteration. In each of the two dimensions there is a preferential direction where the *current* iteration message is propagated while in the opposite direction the *previous* iteration message is propagated. When the preferential direction is left to right, the left-most side of the image has a stronger effect on the result because its message is passed all the way across the image in a single iteration. TRW-S deals with this by alternating the preferential direction. The issue with this solution is that the most extreme elevation angles (far-left and far-right in Fig. 2), where the signal quality is worst, are given the most influence. Since we have the *bottom-bin* in the center of the image and the signal quality is often best in the center, the preference direction was changed to always be outward from the *bottom-bin* ground truth.

4. RESULTS AND DISCUSSION

Table. 1. 2D image tracking error results.

Error	Viterbi [4]	MCMC [5]	Level-sets [3]	Viterbi (Ours)
Mean	43.1	37.4	6.6	6.0
Median	14.4	9.1	2.1	1.0

Table. 2. 3D image tracking error results.

Error	Viterbi	TRW-S	Viterbi (Ours)	TRW-S (Ours)
Mean	12.1	9.7	9.8	5.1
Median	2.0	2.0	1.0	0.0

Above are the results for our modified implementations of the two algorithms, as well as results for previously proposed solutions, in terms of absolute column-wise difference compared to manually detected ground truth, measured in pixels and averaged between all frames analyzed.

We tested our modified Viterbi routine on 2D data from the 2009 NASA Operation IceBridge Antarctica campaign, the same dataset used by the authors of [3] and [5]. The algorithm received no manual aid of any kind, and the only ground-truth provided were the aforementioned crossovers. We did not re-run the other results for the 2D imagery; rather, these are the results published in [3] and [5]. It is crucial to note that previous solutions discarded appreciable amounts of data considered of poor quality or in which the bottom was not clearly visible. We have utilized all segments in which ground-truth data were available; specific sections of the tracking results that present large deviations to the reference have significantly shifted the mean error measurement.

We executed our modified Viterbi and TRW-S implementations on 3D imagery resulting from the 2014 NASA Operation IceBridge Canadian Arctic Archipelago campaign. Previously published results [6] included only 7 frames whereas these results include all 102 frames from the dataset. Regarding these results, it must be noted that the manually detected data were originally tracked using the TRW-S algorithm itself, and therefore the resulting tracked layers may present a bias towards it.

5. ACKNOWLEDGMENTS

Victor Berger, Shane Chu, and John Paden acknowledge support in part by NASA (NNX16AH54G). Mingze Xu, David Crandall, and Geoffrey Fox were supported in part by NSF (1443054). ArcticDEM was provided by the Polar Geospatial Center under NSF OPP awards 1043681, 1559691 and 1542736.

6. REFERENCES

[1] F. Rodríguez-Morales, et. al., "Advanced Multifrequency Radar Instrumentation for Polar Research," IEEE Trans. Geoscience and Remote Sensing, vol. 52, no. 5, May 2014.

[2] C.M. Gifford, G. Finyom, M. Jefferson, Jr., M. Reid, E. L. Akers, and A. Agah, "Automated polar ice thickness estimation from radar imagery", IEEE Trans. Image Process., vol. 19, no. 9, pp. 2456-2469, Sep. 2010.

[3] M. Rahnemoonfar, G. C. Fox, M. Yari and J. Paden, "Automatic Ice Surface and Bottom Boundaries Estimation in Radar Imagery Based on Level-Set Approach," in IEEE Trans. Geosci. Remote Sens., vol. 55, no. 9, pp. 5115-5122, Sept. 2017.

[4] D. J. Crandall, G. C. Fox and J. D. Paden, "Layer-finding in radar echograms using probabilistic graphical models," Proceedings of the 21st International Conference on Pattern Recognition (ICPR2012), Tsukuba, 2012, pp. 1530-1533.

[5] S. Lee, J. Mitchell, D. Crandall, G. Fox, "Estimating bedrock and surface layer boundaries and confidence intervals in ice sheet radar imagery using MCMC," International Conference on Image Processing (ICIP), 2014, pp. 111–115.

[6] M. Xu, D. Crandall, G. Fox, and J. Paden, "Automatic Estimation of Ice Bottom Subsurfaces from Radar Imagery," IEEE International Conference on Image Processing (ICIP), 2017.

[7] V. Kolmogorov, "Convergent tree-reweighted message passing for energy minimization," Transactions on Pattern Analysis and Machine Intelligence, vol.28, no. 10, pp. 1568–1583, 2006.

[8] P. Fretwell, et. al., Bedmap2: improved ice bed, surface and thickness datasets for Antarctica, The Cryo., 7, 375–393, 2013.

[9] J. Paden, T. Akins, D. Dunson, C. Allen, P. Gogineni, "Ice-Sheet Bed 3-D Tomography," J. Glac., vol.56, no.195, pp. 3-11, 2010.

[10] S. Gogineni, et. al., "Bed topography of Jakobshavn Isbræ, Greenland, and Byrd Glacier, Antarctica," J. Glac., vol. 60, no. 223, pp. 813–833, 2014.

[11] A. Arendt, et. al., "Randolph Glacier Inventory [v2.0]: A Dataset of Global Glacier Outlines". Global Land Ice Measurements from Space, Bounder, Colorado, Digital Media, 2012.

[12] J. Bergstra and Y. Bengio, "Random search for hyper-parameter optimization", The Journal of Machine Learning Research, vol.13, pp. 281-305, 2012.

[13] W. Liu, K. Purdon, T. Stafford, J. Paden and X. Li, "Open Polar Server (OPS) – An Open Source Spatial Data Infrastructure for the Cryosphere Community", ISPRS Int. J. Geo-Info., 2016, 5(32).